

# Freak wave statistics on collinear currents

KARINA B. HJELMERVIK AND KARSTEN TRULSEN†

Department of Mathematics, University of Oslo, P.O. Box 1053 Blindern, NO-0316 Oslo, Norway

(Received 23 March 2009; revised 12 May 2009; accepted 20 May 2009; first published online  
17 September 2009)

Linear refraction of waves on inhomogeneous current is known to provoke extreme waves. We investigate the effect of nonlinearity on this phenomenon, with respect to the variation of significant wave height, kurtosis and occurrence of freak waves. Monte Carlo simulations are performed employing a modified nonlinear Schrödinger equation that includes the effects of a prescribed non-potential current. We recommend that freak waves should be defined by a local criterion according to the wave distribution at each location of constant current, not by a global criterion that is either averaged over, or insensitive to, inhomogeneities of the current. Nonlinearity can reduce the modulation of significant wave height. Depending on the configuration of current and waves, the kurtosis and probability of freak waves can either grow or decrease when the wave height increases due to linear refraction. At the centre of an opposing current jet where waves are known to become large, we find that freak waves should be more rare than in the open ocean away from currents. The largest amount of freak waves on an opposing current jet is found at the jet sides where the significant wave height is small.

---

## 1. Introduction

It is well known that linear refraction due to currents can provoke large waves. When waves encounter an opposing current, the wave length can be reduced and both the wave height and steepness can be enhanced. When waves encounter an opposing current jet, focusing can further enhance the wave intensity near the centre of the jet. Linear refraction of waves by currents is known to cause navigational problems, e.g. in the Agulhas current, river estuaries, rip currents, entrances in fjords during outgoing tides and in tidal flows in the coastal zone (Longuet-Higgins & Stewart 1961; Peregrine 1976; González 1984; Jonsson 1990; Lavrenov 1998; Bottin & Thompson 2002; Mori, Liu & Yasuda 2002; MacIver, Simons & Thomas 2006; MacMahan, Thornton & Reniers 2006). When the steepness thus increases, enhanced nonlinear modulations should be anticipated (Stocker & Peregrine 1999; Lavrenov & Porubov 2006). However, it is not well known how the enhanced effect of nonlinearity will modify the wave height.

Our goal is to investigate how nonlinearity modifies both the significant wave height and the occurrence of freak waves, for waves propagating on inhomogeneous stationary currents. Two important reviews of freak waves (Kharif & Pelinovsky 2003; Dysthe, Krogstad & Müller 2008) argue that there is no unique definition of freak waves, but it is generally agreed that they belong to the extreme tail of the probability distribution. The most common definition is that a wave is freak when

† Email address for correspondence: karstent@math.uio.no

the wave height exceeds a threshold related to the significant wave height. However, due to the inhomogeneity of the current, it becomes necessary to distinguish two different types of statistical distributions for the surface waves. In the first case, the distribution is given as a function of location, each location being associated with a constant current, such that the threshold for freak waves will depend on the location. In the second case, a common threshold is defined for the entire domain, either based on an averaging over the entire inhomogeneous domain or based on a reference sea state unaffected by currents and bottom topography.

We argue that, at least when the current is known and stationary, the optimal choice is to use distributions specific to each location, and a freak wave criterion that depends on location. The reason is that freak waves should be surprising, also after the knowledge of the current has been taken into account. Some authors have made the other choice (Lavrenov 1998, and references therein), thus identifying numerous freak waves where large waves should be anticipated in any case.

Laboratory measurements of long-crested waves on a transversally uniform current, show that strong opposing currents induce partial wave blocking significantly elevating the limiting steepness and asymmetry of freak waves (Wu & Yao 2004). MacIver *et al.* (2006) studied waves propagating across a shore-parallel current jet at oblique incidence. They found that a following wave is refracted to a more current-parallel direction with reduced wave height, while an opposing wave becomes more current normal with increased wave height.

Our need to resolve wave phases on non-potential currents restricts us from employing several obvious candidates. White (1999) allowed a prescribed current with vorticity, and derived a wave action equation. Ray theory (White & Fornberg 1998) is used for tracking wave packets. Peregrine & Smith (1979) derived a nonlinear Schrödinger equation useful for caustics where ray theory breaks down. The Zakharov equation (Zakharov 1968) is limited to potential flows.

We shall derive a nonlinear Schrödinger equation that includes an inhomogeneous current with horizontal shear. Some related models have already been published. Stewartson (1977) derived a linear current modified Schrödinger equation to Dysthe level limiting to potential theory. Turpin, Benmoussa & Mei (1983) considered the effects of slowly varying depth and current, and derived a cubic Schrödinger equation limiting to one horizontal dimension. Gerber (1987) used the variational principle to derive a cubic Schrödinger equation for a non-uniform medium, limiting to potential theory in one horizontal dimension. Mei (1989) allowed horizontal shear, and derived the Schrödinger equation to linear order. Stocker & Peregrine (1999) extended the modified nonlinear Schrödinger equation of Dysthe (1979) to include a prescribed potential current induced by for example an internal wave. Our equation will be taken up to cubic nonlinearity, and will include waves and currents in two horizontal dimensions allowing weak horizontal shear.

## 2. The current modified nonlinear Schrödinger equation

Assume that the total velocity field  $\mathbf{v}_{tot} = \mathbf{v} + \mathbf{V}$  is a superposition of the velocity of a wave field  $\mathbf{v} = (u, v, w)$ , and a prescribed stationary current field  $\mathbf{V} = (U, V, W)$  in a Cartesian coordinate system  $(x, y, z)$ . The  $x$ -axis is aligned with the principal propagation direction of the waves. The  $z$ -axis is vertical with unit vector  $\mathbf{k}$  pointing upwards.  $z=0$  corresponds to the undisturbed free water surface. The water is assumed inviscid, incompressible and deep with respect to the characteristic wavelength.

The Euler equation for the combined wave and current field can be written as:

$$\frac{\partial \mathbf{v}}{\partial t} + \mathbf{v}_{tot} \cdot \nabla \mathbf{v}_{tot} = -\frac{1}{\rho} \nabla p_{tot} - g \mathbf{k}. \quad (2.1)$$

The total pressure  $p_{tot} = p_s + p + P$  is a combination of the dynamic pressure due to the wave field  $p$ , the dynamic pressure due to the current field  $P$  and the static pressure  $p_s = -\rho g z + p_a$ , where  $\rho$  is the density,  $g$  is the acceleration of gravity and  $p_a$  is the atmospheric pressure.

The surface boundary equations for the combined field at  $z = \eta + \zeta$  can then be written as:

$$\frac{\partial \eta}{\partial t} + \mathbf{v}_{tot} \cdot \nabla (\eta + \zeta) = w + W, \quad (2.2a)$$

$$p_{tot} = p_a, \quad (2.2b)$$

$\eta$  and  $\zeta$  are the surface displacements associated with the wave field and the current field, respectively.

The vorticity of the waves  $\boldsymbol{\gamma} = \nabla \times \mathbf{v}$  obeys the equation

$$\frac{\partial \boldsymbol{\gamma}}{\partial t} + \mathbf{v}_{tot} \cdot \nabla \boldsymbol{\gamma} - \boldsymbol{\gamma} \cdot \nabla \mathbf{v}_{tot} = -\mathbf{v} \cdot \nabla \boldsymbol{\Gamma} + \boldsymbol{\Gamma} \cdot \nabla \mathbf{v}. \quad (2.3)$$

If the vorticity of the current  $\boldsymbol{\Gamma} = (\Gamma_x, \Gamma_y, \Gamma_z) = \nabla \times \mathbf{V}$  equals zero, (2.3) is homogeneous with respect to  $\boldsymbol{\gamma}$ , and if the wave field starts out irrotational, it will remain irrotational. For waves riding a current field with vorticity, vorticity will develop in the wave field as well. We therefore derive a current modified nonlinear Schrödinger equation that allows a small amount of vorticity.

Let  $a$ ,  $k_c$  and  $\omega_c$  be the characteristic amplitude, wavenumber and angular frequency of the surface waves. We employ the steepness of the waves as a small ordering parameter in the following,  $\epsilon = k_c a \ll 1$ , thus  $k_c \eta = O(\epsilon)$  and  $\mathbf{v} \frac{k_c}{\omega_c} = O(\epsilon)$ . The horizontal current velocities are assumed just small enough to avoid collinear reflection of the waves,  $(U, V)k_c/\omega_c = O(\epsilon)$ . The vertical current velocity is assumed negligible  $Wk_c/\omega_c = O(\epsilon^2)$ . It follows from the Bernoulli equation that the surface displacement induced by the current is small,  $k_c \zeta = O(\epsilon^2)$ . Let the horizontal and vertical length scales  $L$  of the current be longer than a characteristic wavelength so that  $1/(k_c L) = O(\epsilon)$ . The horizontal vorticities  $(\Gamma_x, \Gamma_y)/\omega_c = O(\epsilon^3)$  and the vertical vorticity  $\Gamma_z/\omega_c = O(\epsilon^2)$  are one order smaller than the vorticities assumed by Mei (1989). In the following all equations, variables and sizes are scaled according to the above assumptions, and made dimensionless using the characteristic length and time scales of the wave field.

The wave field is represented by perturbation series for the surface displacement  $\eta$ , the velocity  $\mathbf{v}$  and the pressure  $p$  (see Appendix). The perturbation series for the surface displacement is given by

$$\eta = \epsilon^2 \bar{\eta} + \frac{1}{2} (B e^{i(x-t)} + \epsilon B_2 e^{2i(x-t)} + \epsilon^2 B_3 e^{3i(x-t)} + \dots + \text{c.c.}), \quad (2.4)$$

where  $\bar{\eta}$  is the mean surface displacement,  $x$  is the principal propagation direction and  $B$ ,  $B_2$  and  $B_3$  are the first, second and third harmonics of the surface displacement. We have fixed the characteristic wavenumber appropriate for waves undisturbed by current, therefore the entire effect of refraction is represented by the modulation of  $B$ . The perturbation series for the velocity and the pressure are similar.

Through Taylor expansion around  $z = 0$  and perturbation expansion (see Appendix) we get the following dimensionless Schrödinger equation with current terms, NLSC,

for the first harmonic of the surface elevation of the waves:

$$\frac{\partial B}{\partial x} = (L+C+N)B, \quad (2.5)$$

where  $L$  contains the linear terms with constant coefficients,  $C$  contains the linear terms with variable coefficients and  $N$  is the nonlinear term:

$$\begin{aligned} L &= -2\frac{\partial}{\partial t} - i\frac{\partial^2}{\partial t^2} + \frac{i}{2}\frac{\partial^2}{\partial y^2}, \\ C &= -2iU + 6U\frac{\partial}{\partial t} + 5iU^2 - 2V\frac{\partial}{\partial y} - \frac{\partial U}{\partial x}, \\ N &= -i|B|^2. \end{aligned}$$

Equation (2.5) should be valid for evolution over a distance  $x = O(\epsilon^{-2})$  and for modulations of spectral width  $O(\epsilon)$  in  $y$  and  $t$ .

All the terms in (2.5) may be derived from Stocker & Peregrine (1999) by rescaling their current even though they used potential theory. Our horizontal current is one order stronger, but their equation is of Dysthe order. When vorticity is allowed, new terms will appear if (2.5) is taken to the next order. To obtain (2.5) from (20) in Stocker & Peregrine (1999) one has to recall that the first is written in terms of the free-surface envelope, where as the latter is written in terms of the envelope of the potential.

### 3. Model set-up

Simulations are performed with a second order split-step scheme based on Lo & Mei (1985) and Muslu & Erbay (2004). A Fourier method is used on the linear terms with constant coefficients  $LB$ . And a second-order Runge–Kutta scheme is used on the nonlinear term and the linear terms with variable coefficients  $(C+N)B$ . The wave field is assumed periodic with respect to  $y$  and  $t$ . The integrating step used is  $\Delta x = 0.2$ . Each ensemble consists of 30 simulations.

The Fourier transform with respect to  $y$  and  $t$  is given by

$$\hat{B}_{ij} = \frac{1}{MN} \sum_{m=0}^{M-1} \sum_{n=0}^{N-1} B_{mn} e^{i(\Omega_j t_n - k_{yi} y_m)}, \quad (3.1)$$

where  $y_m = m\Delta y$ ,  $t_n = n\Delta t$ ,  $k_{yi} = i\Delta k_y$  and  $\Omega_j = j\Delta\omega$ . The length of each time series is  $T = 2000$ . Using  $N = 1024$  times, the time step is  $\Delta t = T/N \approx 1.95$  and  $\Delta\omega = 2\pi/T \approx 0.0031$ . The width of the simulation area  $y = [-40, 40]$ , with  $M = 32$  points, gives  $\Delta y = 2.5$  and  $\Delta k_y \approx 0.079$ .

Both unidirectional and short-crested incoming waves with Gaussian spectrum have been studied. The Fourier amplitudes at  $x = 0$  are given respectively by

$$\hat{B}_j = \epsilon \sqrt{\frac{\Delta\omega}{\sqrt{2\pi}\sigma_\omega}} e^{-\frac{\Omega_j^2}{4\sigma_\omega^2} + i\psi_j}, \quad (3.2)$$

$$\hat{B}_{ij} = \epsilon \sqrt{\frac{\Delta k_y \Delta\omega}{2\pi\sigma_y\sigma_\omega}} e^{-\frac{\Omega_j^2}{4\sigma_\omega^2} - \frac{k_{y,i}^2}{4\sigma_y^2} + i\psi_{ij}}. \quad (3.3)$$

The frequency is given by  $\omega_j = 1 + \Omega_j$ . The phases  $\psi_{ij}$  are statistically independent and uniformly distributed on the interval  $[0, 2\pi)$ . We have chosen  $\epsilon = 0.1$ .  $\sigma_\omega$  and

$\sigma_y$  are bandwidths in Fourier room. We have studied  $\sigma_\omega = 0.05, 0.1$  and  $0.2$ . For the short-crested cases we have chosen  $\sigma_y = 0.05$  and  $0.2$  to study different crest lengths.

The NLSC equation (2.5) may be used for a large range of prescribed currents. Here we have chosen two types; a narrow surface current jet (§4.1) given by

$$U = \begin{cases} 0 & \text{when } x \leq X, \text{ and/or } |y| \geq Y \\ U_0 \sin^2\left(\frac{\pi}{2\Delta X}(x - X)\right) \cos^2\left(\frac{\pi y}{2Y}\right) & \text{when } x > X, \text{ and } x < X + \Delta X, \\ U_0 \cos^2\left(\frac{\pi y}{2Y}\right) & \text{when } x \geq X + \Delta X \end{cases} \quad (3.4)$$

and a transversally uniform current (§4.3) given by

$$U = \begin{cases} 0 & \text{when } x \leq X \\ U_0 \sin^2\left(\frac{\pi}{2\Delta X}(x - X)\right) & \text{when } x > X, \text{ and } x < X + \Delta X. \\ U_0 & \text{when } x \geq X + \Delta X \end{cases} \quad (3.5)$$

The wave field is allowed about 32 wavelengths,  $x = [0, X]$  where  $X = 200$ , to develop before it encounters a current.  $Y = 10$  is half the width of the jet. And  $\Delta X = 100$  is the current build-up length. In this paper we compare three cases for the current: no current, cocurrent with  $U_0 = 0.05$  and opposing current with  $U_0 = -0.05$  which is not enough to reflect the waves, but sufficient to study the characteristic features of opposing currents. More current cases are studied in Hjelmervik & Trulsen (2009).

Simulations and observations of tidal currents suggest that establishing current jets are more fanned in than terminating current jets are fanned out (Hjelmervik, Ommundsen & Gjevik 2005). Test simulations show that the current across the jet  $V$ , needed to satisfy the continuity equation, has negligible impact on the results and may thus be set to zero in the NLSC equation. Alternatively, the continuity equation can be satisfied by a vertical current  $W$ , which does not appear within the truncation level of the NLSC equation at the surface.

#### 4. Results

For each of the simulated ensembles we compute the significant wave height  $H_s$ , the kurtosis  $\kappa$ , of the surface displacement and the amount of freak waves from time series at fixed locations. Statistical features are calculated using the envelope to first order. The free surface may be reconstructed to second order by (2.4), using the first harmonic term proportional to  $B$  and the second harmonic term proportional to  $B_2$ . Since the second harmonic complex envelope  $B_2$  is not an explicit function of the current field according to (A 28b), the contribution from bound waves are not expected to modify wave statistics of the free waves differently from the case of no current within the truncation level of (2.5). Second-order harmonic bound contributions without currents are well known from the literature (Longuet-Higgins & Stewart 1961; Tayfun 1980; Socquet-Juglard *et al.* 2005, and others). We shall limit our consideration of wave statistics to contributions from free waves only:

$$H_s(x, y) = 4\sqrt{\overline{\eta^2}} = 4\sqrt{\frac{1}{2}\overline{|B|^2}}, \quad (4.1)$$

$$\kappa(x, y) = \frac{\overline{\eta^4}}{\overline{\eta^2}^2} = \frac{3}{2} \frac{\overline{|B|^4}}{\overline{|B|^2}^2}. \quad (4.2)$$

The overbar represents combined time and ensemble averaging. The significant wave height equals four times the standard deviation of the surface elevation. The kurtosis

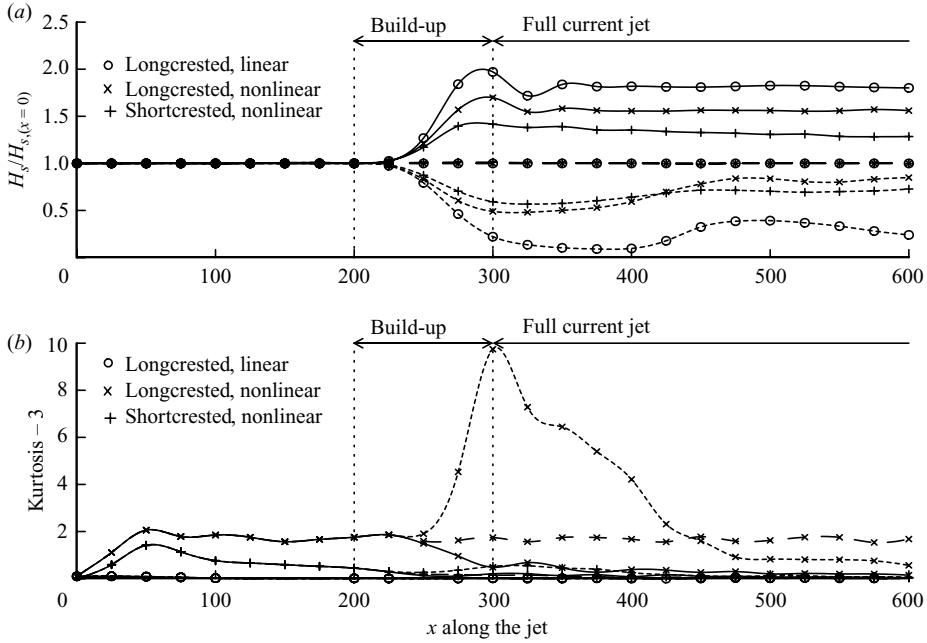


FIGURE 1. The significant wave height (a) and kurtosis (b) with no current (— —), and in the centre of current jets with  $U_0 = -0.05$  (—) and  $0.05$  (- - -) for unidirectional and short-crested ( $\sigma_y = 0.05$ ) incoming waves with  $\sigma_\omega = 0.1$ . For the case of no current, there are three curves on top of each other in (a).

equals three when the surface displacement is Gaussian distributed. We define a wave as freak when its wave height exceeds 2.2 times the significant wave height  $H_s$ :

$$H = 2|B| > 2.2H_s. \tag{4.3}$$

According to the Rayleigh distribution for wave height, 0.006 % of the waves should be freak.

#### 4.1. Current jet

Suppose that the waves meet a collinear surface current jet given by (3.4).

The significant wave height increases for waves encountering an opposing current and decreases for waves encountering a cocurrent (figure 1a). The significant wave height oscillates before stabilizing. Test simulations with wider simulation areas show that the oscillations appearing on the opposing current jet do not depend on the width of the simulation area, but on the width and form of the current jet, while the oscillations after 64 wavelengths ( $x \approx 400$ ) on the cocurrent may be due to restrictions on the simulation area.

The significant wave height is larger in the centre and smaller at the sides of an opposing current jet, while it is smaller in the centre and larger at the sides of a cocurrent jet (figure 2). These results are very similar for different values of  $\sigma_\omega$ , and qualitatively equal for any cross section after the current jet is introduced. When waves encounter an opposing current jet, energy is transferred from the sides of the jet into the centre of the jet resulting in larger significant wave height in the centre of the jet and smaller at the jet sides. More energy is transferred in linear than in nonlinear simulations, and the longer the incoming crest lengths are. When waves encounter a cocurrent jet, the energy is transferred in the opposite direction, resulting

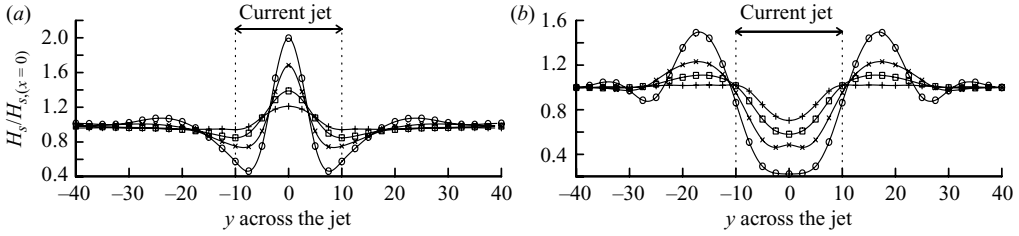


FIGURE 2. The significant wave height at  $x = 300$  across current jets with  $U_0 = -0.05$  (a) and  $0.05$  (b). Unidirectional incoming waves with linear simulations (circle) and nonlinear simulations (cross). Short-crested incoming waves with  $\sigma_y = 0.05$  (square) and  $\sigma_y = 0.2$  (plus) with nonlinear simulations. Incoming  $\sigma_\omega = 0.1$ .

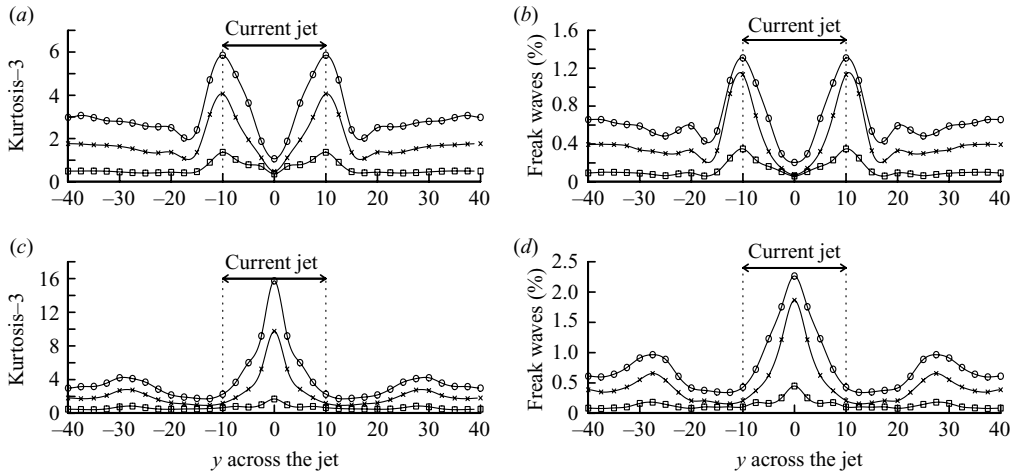


FIGURE 3. The kurtosis (a, c) and amount of local freak waves (b, d) for unidirectional incoming waves at  $x = 300$  across current jets with  $U_0 = -0.05$  (a, b) and  $0.05$  (c, d). Incoming  $\sigma_\omega = 0.05$  (circle),  $0.1$  (cross) and  $0.2$  (square). Nonlinear simulations.

in larger significant wave height at the jet sides and smaller in the centre of the jet. Again more energy is transferred in linear than in nonlinear simulations, and the longer the incoming crest lengths are.

The kurtosis deviates little from three in linear simulations and in nonlinear simulations with short-crested incoming waves (figure 1b). In nonlinear simulations with unidirectional incoming waves, the kurtosis increases to a maximum before decreasing to a stable level. The stable level is reached before the current jet is introduced, and increases with decreasing incoming bandwidth in frequency (figure 3a,c). Simulations with different incoming crest lengths show that larger crest lengths result in larger deviations in the kurtosis both before and shortly after the build-up of the current jet.

When unidirectional waves meet an opposing current jet, the kurtosis decreases in the centre of the jet where the significant wave height grows. The largest kurtosis across the jet is at the sides of the jet where the significant wave height is smallest. When unidirectional waves meet a cocurrent jet, the kurtosis decreases at the sides of the jet where the significant wave height grows. In this case the largest kurtosis is in the centre of the jet where the significant wave height is smallest. Test simulations with different build-up lengths,  $\Delta X = 50, 100, 200$  and  $300$ , show that smaller current

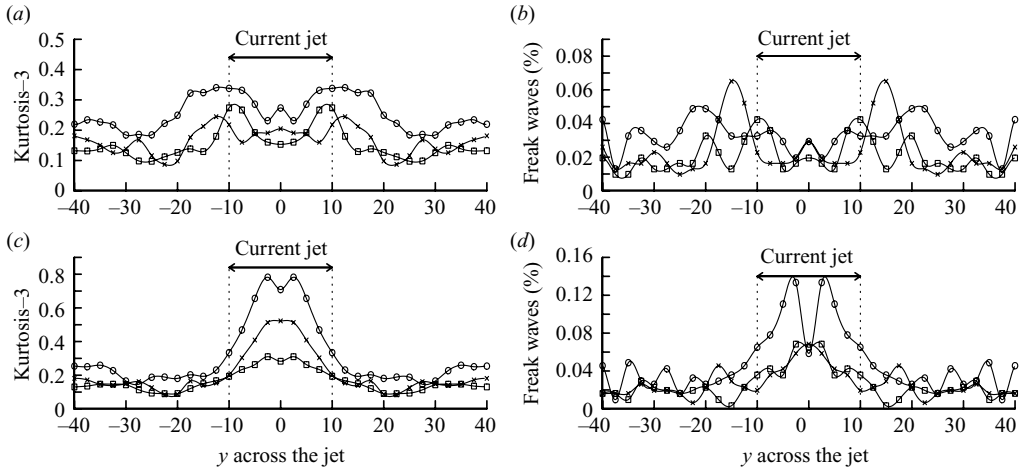


FIGURE 4. The kurtosis (*a, c*) and amount of local freak waves (*b, d*) for incoming short-crested waves ( $\sigma_y = 0.05$ ) at  $x = 300$  across current jets with  $U_0 = -0.05$  (*a, b*) and  $0.05$  (*c, d*). Incoming  $\sigma_\omega = 0.05$  (circle),  $0.1$  (cross) and  $0.2$  (square). Nonlinear simulations.

gradients along the waves  $\partial U/\partial x$  results in smaller changes in the kurtosis along the jet  $|\partial\kappa/\partial x|$  and smaller maximums of the kurtosis across the jet.

Since the current jet is narrower than ten wavelengths, the unidirectional incoming waves behave as short-crested waves (Gramstad & Trulsen 2007) and the kurtosis decreases as the wave field is adjusted to the current jet (figure 1*b*). After the wave field is adjusted to the current jet, the kurtosis is close to three. The significant wave height in the centre of the jet is still large in the opposing current jet and small in the cocurrent jet. The adjustment length of waves without current is well known (Onorato *et al.* 2002; Socquet-Juglard *et al.* 2005; Gramstad & Trulsen 2007). Our numerical results suggest that the adjustment length for waves on collinear current jets can be considerably longer than for waves without currents.

The amount of freak waves is represented well by the kurtosis in our study (figure 3). The largest amount of freak waves is at the sides of the opposing current jet, and in the centre of the cocurrent jet (figure 3*b,d*). Small incoming bandwidths in frequency results in larger maximum of the kurtosis and amount of freak waves, while the significant wave height seems nearly independent of initial bandwidth (Hjelmervik & Trulsen 2009). The waves are large in the centre of an opposing current jet, but the proportion that is freak, is smaller than away from the current. In linear simulations the amount of freak waves is less than 0.04 % at all locations both along and across the jet, but our data material seems to be insufficient to calculate a more exact percentage. In nonlinear simulations with short-crested incoming waves ( $\sigma_y = 0.05$ ) the amount of freak waves is less than 0.15 % (figure 4*b,d*). The longer the incoming crest lengths the larger kurtosis and amount of freak waves. Gramstad & Trulsen (2007) performed a large number of simulations with a modified nonlinear Schrödinger equation in order to reveal how the occurrence of freak waves on deep water depends on crest lengths. They found a clear difference between short-crested and long-crested waves, distinguished by a limiting crest length of approximately ten wavelengths ( $\sigma_y \approx 0.1$ ). Our results indicate that a similar qualitative difference exists when a current jet is introduced. The longer the crest lengths, the stronger the variations in significant wave height, kurtosis and amount of freak waves across the jet.



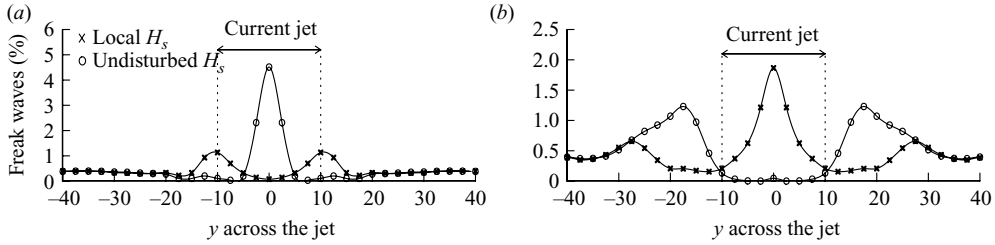


FIGURE 5. The amount of freak waves at  $x = 300$  for unidirectional incoming waves across current jets with  $U_0 = -0.05$  (a) and  $0.05$  (b). Incoming  $\sigma_\omega = 0.1$ . Nonlinear simulations.

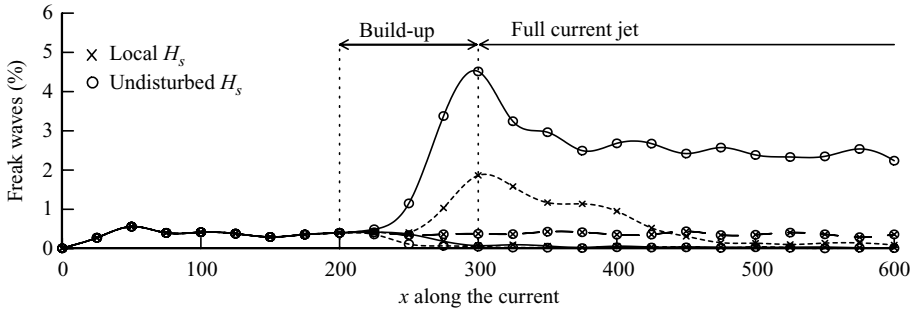


FIGURE 6. The amount of freak waves for unidirectional incoming waves with no current (— —), and in the centre of current jets with  $U_0 = -0.05$  (—) and  $0.05$  (- - -). Incoming  $\sigma_\omega = 0.1$ . Nonlinear simulations.

#### 4.2. Space or time averaged significant wave height

Our definition of freak waves by (4.3) requires knowledge of the significant wave height  $H_s$ . Since the waves propagate in an inhomogeneous medium, there are at least three different strategies for determining  $H_s$ . The strategy which we recommend and have adopted here is to determine  $H_s$  at fixed locations of constant current, i.e. a *local* significant wave height. This method corresponds to classical field measurements taken at fixed locations. A second strategy would be to determine a *global* significant wave height by spatial averaging over the inhomogeneous medium. This method likely corresponds to analysis based on satellite imaging of the ocean surface. A third strategy would be to define an *undisturbed* significant wave height for a wave field unaffected by the inhomogeneities. This method corresponds to the work done by, e.g. Lavrenov (1998).

Lavrenov (1998) considered the propagation of swell from the southern latitudes into the opposing Agulhas current. He found that the mean wave height is larger in the centre of the jet than at the jet sides. Our simulations show that this applies for both linear and nonlinear simulations, and both unidirectional and short-crested incoming waves. He suggested that the amount of freak waves is large in the centre of the jet since the mean wave height is large there.

Figures 5 and 6 show that the amount of ‘freak’ waves strongly depends on the strategy used to define them. The kurtosis is a good indicator for freak waves only if the local significant wave height is used to define them. Then the freak wave amount is large at locations with a large amount of unexpectedly high waves compared to what is expected at the same locations, and when the waves are adjusted to the current jet, the freak wave amount is small. If the undisturbed significant wave height

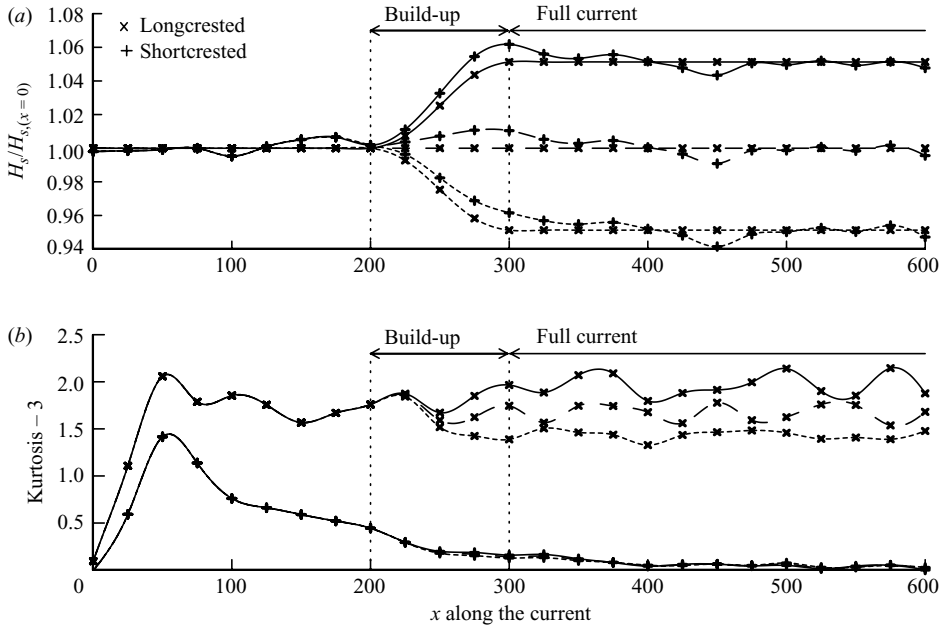


FIGURE 7. The significant wave height (a) and kurtosis (b) for unidirectional and short-crested ( $\sigma_y = 0.05$ ) incoming waves with no current (—), and on transversally uniform currents with  $U_0 = -0.05$  (---) and  $0.05$  (- - -). Incoming  $\sigma_\omega = 0.1$ . Nonlinear simulations.

is used to define the freak waves, the local significant wave height is a good indicator for the freak wave amount. Then the freak wave amount is large at locations with large waves compared to wave heights elsewhere, and when the waves are adjusted to the current jet, the freak wave amount is still large. We believe it is preferable to reserve the term ‘freak’ waves only to those waves that are surprising even after knowledge of inhomogeneities are taken into account. To ensure that a freak wave belongs to the upper tail of the probability distribution, we thus recommend the local significant wave height for application to the criterion (4.3).

#### 4.3. Transversally uniform current

Suppose that the waves meet a transversally uniform current given by (3.5).

The significant wave height (figure 7a) increases when the waves meet an increasing opposing current and decreases when the waves meet an increasing cocurrent. Since the current does not cause any energy transfer transversally, the changes are smaller than when the waves meet a current jet (figure 1a). The significant wave height is near constant after the build-up of the current.

The kurtosis (figure 7b) for long-crested waves increases slightly when the significant wave height increases, and decreases slightly when the significant wave height decreases. This effect can hardly be seen for short-crested waves. After the current build-up the unidirectional incoming waves are still unidirectional and the kurtosis stays at the same level. This is in contradiction to the case where unidirectional incoming waves meet a current jet (figure 1b). Then the kurtosis decreases with increasing significant wave height, increases with decreasing significant wave height, and decreases after the build-up. The kurtosis for unidirectional incoming waves with no current (figures 1b and 7b) stays at a high level, indicating that the cubic nonlinear Schrödinger equation produces larger kurtosis than the modified Schrödinger equation

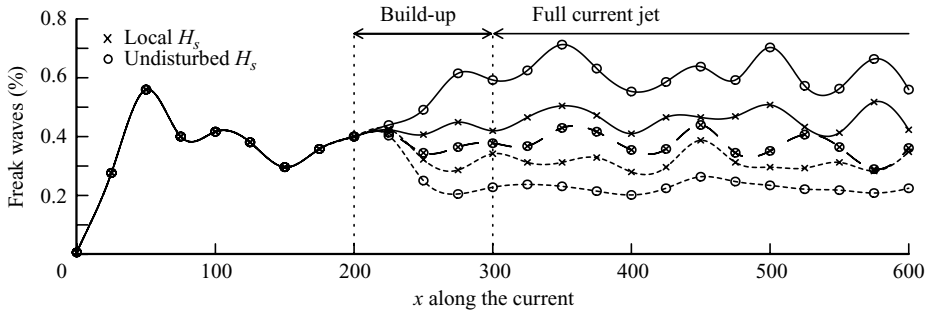


FIGURE 8. The amount of freak waves for unidirectional incoming waves with no current (— —), and on transversally uniform currents with  $U_0 = -0.05$  (— —) and  $0.05$  (- - -). Incoming  $\sigma_\omega = 0.1$ . Nonlinear simulations.

by Trulsen & Dysthe (1996) derived to next order (see Gramstad & Trulsen 2007, figure 2).

On a transversally uniform current the amount of freak waves (figure 8) is well indicated by the kurtosis also when the undisturbed significant wave height is used to calculate the amount of freak waves. If the undisturbed significant wave height is used, there are slightly more freak waves in an opposing current and less in a cocurrent, than if the local significant wave height is used. Since the current does not introduce transversal energy transfer, the freak wave amounts are smaller than if the waves meet a current jet (figure 5).

## 5. Conclusion

We have derived a nonlinear Schrödinger equation suitable for spatial wave propagation on inhomogeneous currents. We have used this equation for Monte Carlo simulations to investigate wave statistics on inhomogeneous currents, in particular on narrow current jets. Several surprising features of nonlinear wave evolution on nonuniform current were revealed. Wave statistics has been derived based on the envelope to the first order, which was used to estimate the wave height correct to second order.

The evolution and statistics of both short- and long-crested waves on transversally uniform currents is found to be qualitatively different from waves on current jets.

Considering waves that approach an opposing current jet, we find that the amount of freak waves is minimum in the centre of the jet where the wave heights are largest, while the amount of freak waves is maximum at the sides of the jet where the wave heights are smallest.

The definition of both significant wave height and of freak waves can be ambiguous in inhomogeneous media. We recommend that *local* definitions are used to ensure that freak waves remain surprising even after classical knowledge of the inhomogeneous medium has been taken into account.

We see evidence that the distances over which a wave field has to propagate in order to be adjusted to the medium can become much longer in the presence of inhomogeneous currents than in the absence of currents. This may be an important consideration for the appropriate choice of wave models in coastal waters.

We thank professors Kristian B. Dysthe and Bjørn Gjevik for fruitful discussions. Several referees provided useful comments on preliminary versions of the manuscript.

Karsten Trulsen is grateful for the hospitality of the Department of Signal Theory and Communications at the Polytechnic School at the University of Alcalá, Spain, for hosting him during a sabbatical year during the development of this paper.

### Appendix. Derivation of the NLSC equation

Taylor expansions around  $z=0$  gives the surface boundary equations, (2.2a–b), on the form:

$$\begin{aligned} \frac{\partial \eta}{\partial t} + \mathbf{v}_{tot} \cdot \nabla(\eta + \zeta) + (\eta + \zeta) \frac{\partial \mathbf{v}_{tot}}{\partial z} \cdot \nabla(\eta + \zeta) + \frac{1}{2}(\eta + \zeta)^2 \frac{\partial^2 \mathbf{v}_{tot}}{\partial z^2} \cdot \nabla(\eta + \zeta) \\ = w + W + (\eta + \zeta) \frac{\partial}{\partial z}(w + W) + \frac{1}{2}(\eta + \zeta) \frac{\partial^2}{\partial z^2}(w + W) + \dots, \end{aligned} \quad (\text{A } 1a)$$

$$p_{tot} + (\eta + \zeta) \frac{\partial p_{tot}}{\partial z} + \frac{1}{2}(\eta + \zeta)^2 \frac{\partial^2 p_{tot}}{\partial z^2} + \dots = p_a. \quad (\text{A } 1b)$$

The waves are assumed on deep water, that is,  $\mathbf{v}, p \rightarrow 0$  as  $z \rightarrow -\infty$ .

In accordance with the scaling assumptions from §2, all equations, variables and sizes in the following are made dimensionless using the characteristic length and time scales of the wave field, so that  $k_c \mathbf{x} \rightarrow \mathbf{x}$ ,  $\epsilon k_c \mathbf{x} \rightarrow \bar{\mathbf{x}}$ ,  $\omega_c t \rightarrow t$ ,  $k_c \eta \rightarrow \epsilon \eta$ ,  $k_c \zeta \rightarrow \epsilon^2 \zeta$ ,  $\frac{k_c}{\omega_c} \mathbf{u} \rightarrow \epsilon \mathbf{u}$ ,  $\frac{k_c}{\omega_c}(U, V) \rightarrow \epsilon(U, V)$ ,  $\frac{k_c}{\omega_c} W \rightarrow \epsilon^2 W$ ,  $\frac{k_c}{\rho g} p \rightarrow \epsilon p$  and  $\frac{k_c}{\rho g} P \rightarrow \epsilon^2 P$ .

The scaled Euler equation for the waves (2.1) to the third order of  $\epsilon$  is

$$\frac{\partial u}{\partial t} + \epsilon \left( U \frac{\partial u}{\partial x} + V \frac{\partial u}{\partial y} + \mathbf{v} \cdot \nabla u \right) + \epsilon^2 \left( u \frac{\partial U}{\partial \bar{x}} + v \frac{\partial U}{\partial \bar{y}} + W \frac{\partial u}{\partial z} \right) = -\frac{\partial p}{\partial x}, \quad (\text{A } 2a)$$

$$\frac{\partial v}{\partial t} + \epsilon \left( U \frac{\partial v}{\partial x} + V \frac{\partial v}{\partial y} + \mathbf{v} \cdot \nabla v \right) + \epsilon^2 \left( u \frac{\partial V}{\partial \bar{x}} + v \frac{\partial V}{\partial \bar{y}} + W \frac{\partial v}{\partial z} \right) = -\frac{\partial p}{\partial y}, \quad (\text{A } 2b)$$

$$\frac{\partial w}{\partial t} + \epsilon \left( U \frac{\partial w}{\partial x} + V \frac{\partial w}{\partial y} + \mathbf{v} \cdot \nabla w \right) + \epsilon^2 W \frac{\partial w}{\partial z} = -\frac{\partial p}{\partial z}. \quad (\text{A } 2c)$$

The scaled equation for the divergence of the Euler equation for the waves (2.1) to the third order of  $\epsilon$  is

$$\begin{aligned} \epsilon \left( \left( \frac{\partial u}{\partial x} \right)^2 + \left( \frac{\partial v}{\partial y} \right)^2 + \left( \frac{\partial w}{\partial z} \right)^2 + 2 \frac{\partial u}{\partial y} \frac{\partial v}{\partial x} + 2 \frac{\partial u}{\partial z} \frac{\partial w}{\partial x} + 2 \frac{\partial v}{\partial z} \frac{\partial w}{\partial y} \right) \\ + 2\epsilon^2 \left( \frac{\partial u}{\partial x} \frac{\partial U}{\partial \bar{x}} + \frac{\partial u}{\partial y} \frac{\partial V}{\partial \bar{x}} + \frac{\partial v}{\partial x} \frac{\partial U}{\partial \bar{y}} + \frac{\partial v}{\partial y} \frac{\partial V}{\partial \bar{y}} \right) = -\frac{\partial^2 p}{\partial x^2} - \frac{\partial^2 p}{\partial y^2} - \frac{\partial^2 p}{\partial z^2}. \end{aligned} \quad (\text{A } 3)$$

The scaled surface equations for the waves (A 1a–b) to the third order of  $\epsilon$  are

$$\frac{\partial \eta}{\partial t} + \epsilon(\mathbf{v} + \mathbf{V}) \cdot \nabla \eta + \epsilon^2 \eta \frac{\partial \mathbf{v}}{\partial z} \cdot \nabla \eta = w + \epsilon \eta \frac{\partial w}{\partial z} + \epsilon^2 \left( \zeta \frac{\partial w}{\partial z} + \frac{1}{2} \eta^2 \frac{\partial^2 w}{\partial z^2} \right), \quad (\text{A } 4a)$$

$$p - \eta + \epsilon \eta \frac{\partial p}{\partial z} + \epsilon^2 \left( \zeta \frac{\partial p}{\partial z} + \frac{1}{2} \eta^2 \frac{\partial^2 p}{\partial z^2} \right) = 0. \quad (\text{A } 4b)$$

The wave field is represented by perturbation series for the surface displacement  $\eta$ , the velocity  $\mathbf{v}$  and the dynamic pressure  $p$ :

$$\left. \begin{aligned} \eta &= \epsilon^2 \bar{\eta} + \frac{1}{2} (B_1 e^{i(x-t)} + \epsilon B_2 e^{2i(x-t)} + \dots + \text{c.c.}) \\ \mathbf{v} &= \epsilon^2 \bar{\mathbf{v}} + \frac{1}{2} (\mathbf{v}_1 e^{i(x-t)} + \epsilon \mathbf{v}_2 e^{2i(x-t)} + \dots + \text{c.c.}) \\ p &= \epsilon \bar{p} + \frac{1}{2} (p_1 e^{i(x-t)} + \epsilon p_2 e^{2i(x-t)} + \dots + \text{c.c.}) \end{aligned} \right\}. \quad (\text{A } 5)$$

We shall assume that the waves are modulated on the slow spatial scales  $\bar{x}$  and  $\bar{y}$  and a correspondingly slow time scale  $\epsilon t = \bar{t}$ . Thus  $\bar{\eta} = \bar{\eta}(\bar{x}, \bar{y}, \bar{t})$ ,  $\bar{\mathbf{v}} = \bar{\mathbf{v}}(\bar{x}, \bar{y}, z, \bar{t})$ , and  $\bar{p} = \bar{p}(\bar{x}, \bar{y}, z, \bar{t})$  are the mean surface displacement, mean induced velocity and mean dynamic pressure respectively, while  $B_n = B_n(\bar{x}, \bar{y}, \bar{t})$ ,  $\mathbf{v}_n = \mathbf{v}_n(\bar{x}, \bar{y}, z, \bar{t})$  and  $p_n = p_n(\bar{x}, \bar{y}, z, \bar{t})$  are the  $n$ th harmonics of the surface displacement, induced current and dynamic pressure, respectively. The characteristic wavenumber is fixed appropriate for waves undisturbed by current, therefore the entire effect of refraction is represented by the modulation of  $B_1$ .

The horizontal vorticities and the vertical vorticity are all one order higher than the vorticities used by Mei (1989), that is,  $(\Gamma_x, \Gamma_y) = O(\epsilon^3)$  and  $\Gamma_z = O(\epsilon^2)$ . Since the vorticity is assumed to be small, the chosen order of the mean functions are supported by Dysthe (1979). Both the mean functions and the harmonics, are perturbed:

$$\left. \begin{aligned} \bar{\eta} &= \bar{\eta}_2 + \dots, & B_n &= B_{n0} + \epsilon B_{n1} + \epsilon^2 B_{n2} + \dots \\ \bar{\mathbf{v}} &= \bar{\mathbf{v}}_2 + \dots, & \mathbf{v}_n &= \mathbf{v}_{n0} + \epsilon \mathbf{v}_{n1} + \epsilon^2 \mathbf{v}_{n2} + \dots \\ \bar{p} &= \bar{p}_1 + \epsilon \bar{p}_2 + \dots, & p_n &= p_{n0} + \epsilon p_{n1} + \epsilon^2 p_{n2} + \dots \end{aligned} \right\} \quad (\text{A } 6)$$

A.1. First-order terms

The first harmonic terms of first order of  $\epsilon$  for the divergence of the Euler equation (A 3) are

$$p_{10} - \frac{\partial^2 p_{10}}{\partial z^2} = 0, \quad (\text{A } 7)$$

which has the general solution

$$p_{10} = A_{10}(\bar{x}, \bar{y}, \bar{t})e^z. \quad (\text{A } 8)$$

The first harmonic terms of first order of  $\epsilon$  in the surface equations (A 4a–b) give

$$A_{10} = B_{10}. \quad (\text{A } 9)$$

The first harmonic terms of first order of  $\epsilon$  in the Euler equation (A 2a–c) then give, respectively,

$$u_{10} = B_{10}e^z, \quad (\text{A } 10a)$$

$$v_{10} = 0, \quad (\text{A } 10b)$$

$$w_{10} = -iB_{10}e^z. \quad (\text{A } 10c)$$

A.2. Second-order terms

A.2.1. Zeroth harmonic

The zeroth harmonic terms of second order of  $\epsilon$  for the  $z$  component of the Euler equation (A 2c) are

$$\frac{i}{4}u_{10}w_{10}^* + \frac{i}{4}u_{10}^*w_{10} + \frac{1}{4}w_{10}\frac{\partial w_{10}^*}{\partial z} + \frac{1}{4}w_{10}^*\frac{\partial w_{10}}{\partial z} = -\frac{\partial \bar{p}_1}{\partial z}. \quad (\text{A } 11)$$

Using the results (A 10) from first order, gives

$$|B_{10}|^2 e^{2z} = -\frac{\partial \bar{p}_1}{\partial z}, \quad (\text{A } 12)$$

which has the solution

$$\bar{p}_1 = \bar{A}_1(\bar{x}, \bar{y}, \bar{t}) - \frac{1}{2}|B_{10}|^2 e^{2z}. \quad (\text{A } 13)$$

The zeroth harmonic terms of second order of  $\epsilon$  in the dynamic surface equation (A 4b) are

$$\bar{p}_1 + \frac{1}{4}B_{10} \frac{\partial p_{10}^*}{\partial z} + \frac{1}{4}B_{10}^* \frac{\partial p_{10}}{\partial z} = 0, \quad \text{at } z=0. \quad (\text{A } 14)$$

Using the results (A 8–A 9) from first order and the solution for  $\bar{p}_1$  (A 13), gives  $\bar{A}_1 = 0$ .

### A.2.2. First harmonic

The first harmonic terms of second order of  $\epsilon$  for the divergence of the Euler equation (A 3) are

$$2i \frac{\partial p_{10}}{\partial \bar{x}} = p_{11} - \frac{\partial^2 p_{11}}{\partial z^2}. \quad (\text{A } 15)$$

Using the results (A 8–A 9) from leading order, gives

$$2i \frac{\partial B_{10}}{\partial \bar{x}} e^z = p_{11} - \frac{\partial^2 p_{11}}{\partial z^2}, \quad (\text{A } 16)$$

which has the solution

$$p_{11} = A_{11}(\bar{x}, \bar{y}, \bar{t}) e^z - i \frac{\partial B_{10}}{\partial \bar{x}} z e^z. \quad (\text{A } 17)$$

The first harmonic terms of second order of  $\epsilon$  in the dynamic surface equation (A 4b) give

$$A_{11} = B_{11}. \quad (\text{A } 18)$$

The first harmonic terms of second order of  $\epsilon$  in the Euler equation and the kinematic surface equation (A 2a–c, A 4a) are, respectively,

$$\frac{\partial u_{10}}{\partial \bar{t}} - i u_{11} + i u_{10} U = - \frac{\partial p_{10}}{\partial \bar{x}} - i p_{11}, \quad (\text{A } 19a)$$

$$\frac{\partial v_{10}}{\partial \bar{t}} - i v_{11} + i v_{10} U = - \frac{\partial p_{10}}{\partial \bar{y}}, \quad (\text{A } 19b)$$

$$\frac{\partial w_{10}}{\partial \bar{t}} - i w_{11} + i w_{10} U = - \frac{\partial p_{11}}{\partial z}, \quad (\text{A } 19c)$$

$$\frac{\partial B_{10}}{\partial \bar{t}} - i B_{11} + i U B_{10} = w_{11}, \quad \text{at } z=0. \quad (\text{A } 19d)$$

Using the results (A 8)–(A 10) from first order and the solution for  $p_{11}$  (A 17)–(A 18), leads to the current modified Schrödinger equation to second order

$$\frac{\partial B_{10}}{\partial \bar{x}} + 2 \frac{\partial B_{1,0}}{\partial \bar{t}} + 2i U B_{10} = 0, \quad (\text{A } 20)$$

and the reconstruction formulas

$$u_{11} = B_{11}e^z + i \left( \frac{\partial B_{10}}{\partial \bar{t}} + iU B_{10} \right) (1 + 2z)e^z, \quad (\text{A } 21a)$$

$$v_{11} = -i \frac{\partial B_{10}}{\partial \bar{y}} e^z, \quad (\text{A } 21b)$$

$$w_{11} = -iB_{11}e^z + \left( \frac{\partial B_{10}}{\partial \bar{t}} + iU B_{10} \right) (1 + 2z)e^z. \quad (\text{A } 21c)$$

### A.2.3. Second harmonic

The second harmonic terms of second order of  $\epsilon$  for the divergence of the Euler equation (A 3) are

$$-\frac{1}{2}u_{10}^2 + \frac{1}{2} \left( \frac{\partial w_{10}}{\partial z} \right)^2 + i \frac{\partial u_{10}}{\partial z} w_{10} = 4p_{20} - \frac{\partial^2 p_{20}}{\partial z^2}. \quad (\text{A } 22)$$

Using the results (A 10) from leading order, gives

$$0 = 4p_{20} - \frac{\partial^2 p_{20}}{\partial z^2}, \quad (\text{A } 23)$$

which has the solution

$$p_{20} = A_{20}e^{2z}. \quad (\text{A } 24)$$

The second harmonic terms of second order of  $\epsilon$  in the dynamic surface equation (A 4b) are

$$p_{20} - B_{20} + \frac{1}{2}B_{10} \frac{\partial p_{10}}{\partial z} = 0, \quad \text{at } z = 0. \quad (\text{A } 25)$$

Using the results (A 8)–(A 9) from leading order and the solution for  $p_{20}$  (A 24), gives:

$$A_{20} = B_{20} - \frac{1}{2}B_{10}^2. \quad (\text{A } 26)$$

The second harmonic terms of second order of  $\epsilon$  in the Euler equation and the kinematic surface equation (A 2a–c), (A 4) are, respectively,

$$-iu_{20} + \frac{i}{4}u_{10}^2 + \frac{1}{4}w_{10} \frac{\partial u_{10}}{\partial z} = -ip_{20}, \quad (\text{A } 27a)$$

$$-iv_{20} + \frac{i}{4}u_{10}v_{10} + \frac{1}{4}w_{10} \frac{\partial v_{10}}{\partial z} = 0, \quad (\text{A } 27b)$$

$$-iw_{20} + \frac{i}{4}u_{10}w_{10} + \frac{1}{4}w_{10} \frac{\partial w_{10}}{\partial z} = -\frac{1}{2} \frac{\partial p_{20}}{\partial z}, \quad (\text{A } 27c)$$

$$-iB_{20} + \frac{i}{4}u_{10} = \frac{1}{2}w_{20} + \frac{1}{4}B_{10} \frac{\partial w_{10}}{\partial z}, \quad \text{at } z = 0. \quad (\text{A } 27d)$$

Using the results (A 10) from first order and the solution for  $p_{20}$  (A 24), (A 26), gives

$$u_{20} = v_{20} = w_{20} = p_{20} = 0, \quad (\text{A } 28a)$$

$$B_{20} = \frac{1}{2}B_{10}^2. \quad (\text{A } 28b)$$

Note that the second-order contributions is not explicit functions of the current field.

## A.3. Third-order terms

The first harmonic terms of third order of  $\epsilon$  for the divergence of the Euler equation (A 3) are

$$\begin{aligned} u_{20}u_{10}^* + \frac{1}{2} \frac{\partial w_{20}}{\partial z} \frac{\partial w_{10}^*}{\partial z} - \frac{i}{2} \frac{\partial u_{20}}{\partial z} w_{10}^* + i \frac{\partial u_{10}^*}{\partial z} w_{20} + i u_{10} \frac{\partial U}{\partial \bar{x}} + i v_{10} \frac{\partial U}{\partial \bar{y}} \\ = -\frac{1}{2} \frac{\partial^2 p_{10}}{\partial \bar{x}^2} - i \frac{\partial p_{11}}{\partial \bar{x}} + \frac{1}{2} p_{12} - \frac{1}{2} \frac{\partial^2 p_{10}}{\partial \bar{y}^2} - \frac{1}{2} \frac{\partial^2 p_{12}}{\partial z^2}. \end{aligned} \quad (\text{A } 29)$$

Using the results (A 8)–(A 10), (A 17)–(A 18), (A 28) from first and second order, gives

$$\frac{\partial^2 p_{12}}{\partial z^2} - p_{12} = -2i \frac{\partial B_{11}}{\partial \bar{x}} e^z - \frac{\partial^2 B_{10}}{\partial \bar{x}^2} e^z - \frac{\partial^2 B_{10}}{\partial \bar{y}^2} e^z - 2 \frac{\partial^2 B_{10}}{\partial \bar{x}^2} z e^z - 2i B_{10} \frac{\partial U}{\partial \bar{x}} e^z, \quad (\text{A } 30)$$

which has the solution

$$p_{1,2} = A_{12}(\bar{x}, \bar{y}, \bar{z}, \bar{t}) e^z + \alpha(\bar{x}, \bar{y}, \bar{z}, \bar{t}) z e^z + \beta(\bar{x}, \bar{y}, \bar{t}) z^2 e^z, \quad (\text{A } 31)$$

where

$$\begin{aligned} \alpha &= -i \frac{\partial B_{11}}{\partial \bar{x}} - \frac{1}{2} \frac{\partial^2 B_{10}}{\partial \bar{y}^2} - i B_{10} \frac{\partial U}{\partial \bar{x}}, \\ \beta &= -\frac{1}{2} \frac{\partial^2 B_{10}}{\partial \bar{x}^2}. \end{aligned}$$

The first harmonic terms of third order of  $\epsilon$  in the dynamic surface equation (A 4b) are

$$\begin{aligned} \frac{1}{2} p_{12} - \frac{1}{2} B_{12} + \frac{1}{4} B_{20} \frac{\partial p_{10}^*}{\partial z} + \frac{1}{4} B_{10}^* \frac{\partial p_{20}}{\partial z} + \frac{1}{2} B_{10} \frac{\partial \bar{p}_1}{\partial z} \\ + \frac{1}{2} \zeta \frac{\partial p_{10}}{\partial z} + \frac{1}{16} B_{10}^2 \frac{\partial^2 p_{10}^*}{\partial z^2} + \frac{1}{8} |B_{10}|^2 \frac{\partial^2 p_{10}}{\partial z^2} = 0, \quad \text{at } z = 0. \end{aligned} \quad (\text{A } 32)$$

Using the results (A 8)–(A 9), (A 13), (A 28)–(A 28) from first and second order, and the solution for  $p_{12}$  (A 31), gives

$$A_{12} = B_{12} + \frac{3}{8} B_{10}^2 B_{10}^* - B_{10} \zeta, \quad \text{at } z = 0. \quad (\text{A } 33)$$

The first harmonic terms of third order of  $\epsilon$  in the Euler equation and the kinematic surface equation (A 2a–c), (A 4a) are, respectively,

$$\begin{aligned} \frac{1}{2} \frac{\partial u_{11}}{\partial \bar{t}} - \frac{i}{2} u_{12} + \frac{1}{2} \frac{\partial u_{10}}{\partial \bar{x}} U + \frac{i}{2} u_{11} U + \frac{1}{2} \frac{\partial u_{10}}{\partial \bar{y}} V + \frac{1}{2} u_{10} W + \frac{1}{2} u_{10} \frac{\partial U}{\partial \bar{x}} + \frac{1}{2} v_{10} \frac{\partial U}{\partial \bar{y}} \\ - \frac{i}{4} u_{20} u_{1,0}^* + \frac{i}{2} u_{10}^* u_{20} + \frac{1}{4} w_{20} \frac{\partial u_{10}^*}{\partial z} + \frac{1}{4} w_{10}^* \frac{\partial u_{20}}{\partial z} = -\frac{1}{2} \frac{\partial p_{11}}{\partial \bar{x}} - \frac{i}{2} p_{12}, \end{aligned} \quad (\text{A } 34a)$$

$$\begin{aligned} \frac{1}{2} \frac{\partial v_{11}}{\partial \bar{t}} - \frac{i}{2} v_{12} + \frac{1}{2} \frac{\partial v_{10}}{\partial \bar{x}} U + \frac{i}{2} v_{11} U + \frac{1}{2} \frac{\partial v_{10}}{\partial \bar{y}} V + \frac{1}{2} v_{10} W + \frac{1}{2} u_{10} \frac{\partial V}{\partial \bar{x}} + \frac{1}{2} v_{10} \frac{\partial V}{\partial \bar{y}} \\ - \frac{i}{4} u_{20} v_{1,0}^* + \frac{i}{2} u_{10}^* v_{20} + \frac{1}{4} w_{20} \frac{\partial v_{10}^*}{\partial z} + \frac{1}{4} w_{10}^* \frac{\partial v_{20}}{\partial z} = -\frac{1}{2} \frac{\partial p_{11}}{\partial \bar{y}}, \end{aligned} \quad (\text{A } 34b)$$

$$\begin{aligned} \frac{1}{2} \frac{\partial w_{11}}{\partial \bar{t}} - \frac{i}{2} w_{12} + \frac{1}{2} \frac{\partial w_{10}}{\partial \bar{x}} U + \frac{i}{2} w_{11} U + \frac{1}{2} \frac{\partial w_{10}}{\partial \bar{y}} V + \frac{1}{2} w_{10} W \\ - \frac{i}{4} u_{20} w_{1,0}^* + \frac{i}{2} u_{10}^* w_{20} + \frac{1}{4} w_{20} \frac{\partial w_{10}^*}{\partial z} + \frac{1}{4} w_{10}^* \frac{\partial w_{20}}{\partial z} = -\frac{1}{2} \frac{\partial p_{12}}{\partial z}, \end{aligned} \quad (\text{A } 34c)$$



$$\begin{aligned} & \frac{1}{2} \frac{\partial B_{11}}{\partial \bar{t}} - \frac{i}{2} B_{12} - \frac{i}{4} u_{20} B_{10}^* + \frac{i}{2} u_{10}^* B_{20} + \frac{i}{2} B_{11} U + \frac{1}{2} \frac{\partial B_{10}}{\partial \bar{x}} U + \frac{1}{2} \frac{\partial B_{10}}{\partial \bar{y}} V + \frac{i}{8} B_{10}^2 \frac{\partial u_{10}^*}{\partial z} \\ & = \frac{1}{2} w_{12} + \frac{1}{4} B_{20} \frac{\partial w_{10}^*}{\partial z} + \frac{1}{2} B_{10}^* \frac{\partial w_{20}}{\partial z} + \frac{1}{2} \zeta \frac{\partial w_{10}}{\partial z} + \frac{1}{16} B_{10}^2 \frac{\partial w_{10}^*}{\partial z} \\ & + \frac{1}{8} |B_{10}|^2 \frac{\partial^2 w_{10}}{\partial z^2}, \quad \text{at } z = 0. \end{aligned} \tag{A 34d}$$

Combining these equations with the results (A 10), (A 17)–(A 18), (A 21), (A 28) from first and second order, and the solution for  $p_{12}$  (A 31, A 33), gives

$$\begin{aligned} 0 = & \frac{\partial B_{11}}{\partial \bar{x}} + 2 \frac{\partial B_{11}}{\partial \bar{t}} + i \frac{\partial^2 B_{10}}{\partial \bar{t}^2} - \frac{i}{2} \frac{\partial^2 B_{10}}{\partial \bar{y}^2} + i B_{10}^2 B_{10}^* \\ & + 2i B_{11} U - 6 \frac{\partial B_{10}}{\partial \bar{t}} U - 5i B_{10} U^2 + 2 \frac{\partial B_{10}}{\partial \bar{y}} V + B_{10} \frac{\partial U}{\partial \bar{x}}, \end{aligned} \tag{A 35}$$

which combined with (A 20) leads to the space evolution of the current modified cubic nonlinear Schrödinger equation, NLSC, (2.5) where  $B = B_1$  and the bars are dropped to simplify the notation.

More on the derivation of the NLSC equation can be found in Hjelmervik & Trulsen (2009).

#### REFERENCES

- BOTTIN, R. R., JR. & THOMPSON, E. F. 2002 Comparisons of physical and numerical model wave predictions with prototype data at Morro Bay harbor entrance, ERDC/CHL CHETN I-65, U.S. Army Engineer Research and Development Center, Vicksburg, MS.
- DYSTHE, K. B. 1979 Note on the modification to the nonlinear Schrödinger equation for application to deep water waves. *Proc. R. Soc. Lond. A* **369**, 105–114.
- DYSTHE, K. B., KROGSTAD, H. E. & MÜLLER, P. 2008 Oceanic rogue waves. *Annu. Rev. Fluid Mech.* **40**, 287–310.
- GERBER, M. 1987 The Benjamin–Feir instability of a deep water Stokes wavepacket in the presence of a non-uniform medium. *J. Fluid Mech.* **176**, 311–332.
- GONZÁLEZ, F. I. 1984 A case study of wave–current–bathymetry interactions at the Columbia river entrance. *J. Phys. Oceanogr.* **14**, 1065–1078.
- GRAMSTAD, O. & TRULSEN, K. 2007 Influence of crest and group length on the occurrence of freak waves. *J. Fluid Mech.* **582**, 463–472.
- HJELMERVIK, K., OMMUNDSEN, A. & GJEVIK, B. 2005 Implementation of non-linear advection terms in a high resolution tidal model. University of Oslo, Preprint.
- HJELMERVIK, K. & TRULSEN, K. 2009 The current modified nonlinear Schrödinger equation which allows vorticity. University of Oslo, Preprint.
- JONSSON, I. G. 1990 Wave–current interactions. In *The Sea: Ocean Engineering Science* (ed. B. Le Mhauté & D. M. Hanes), pp. 65–120. Wiley-Interscience.
- KHARIF, C. & PELINOVSKY, E. 2003 Physical mechanisms of the rogue wave phenomenon. *Eur. J. Mech. B/Fluids* **22**, 603–634.
- LAVRENOV, I. V. 1998 The wave energy concentration at the Agulhas current off South Africa. *Nat. Hazards* **17**, 117–127.
- LAVRENOV, I. V. & PORUBOV, A. V. 2006 Three reasons for freak wave generation in the non-uniform current. *Eur. J. Mech. B/Fluids* **25**, 574–585.
- LO, E. Y. & MEI, C. C. 1985 A numerical study of water–wave modulation based on a higher-order nonlinear Schrödinger equation. *J. Fluid Mech.* **150**, 395–416.
- LONGUET-HIGGINS, M. S. & STEWART, R. W. 1961 The changes in amplitude of short gravity waves on steady non-uniform currents. *J. Fluid Mech.* **10**, 529–549.
- MACIVER, R. D., SIMONS, R. R. & THOMAS, G. P. 2006 Gravity waves interacting with narrow jet-like current. *J. Geophys. Res.* **111**, C03009.

- MACMAHAN, J. H., THORNTON, E. B. & RENIERS, A. J. H. M. 2006 Rip current review. *Coast. Engng* **53**, 191–208.
- MEI, C. C. 1989 *The Applied Dynamics of Ocean Surface Waves*. World Scientific.
- MORI, N., LIU, P. C. & YASUDA, T. 2002 Analysis of freak wave measurements in the sea of Japan. *Ocean Engng* **29**, 1399–1414.
- MUSLU, G. M. & ERBAY, H. A. 2004 Higher-order split-step Fourier schemes for the generalized nonlinear Schrödinger equation. *Math. Comput. Simul.* **67**, 581–595.
- ONORATO, M., OSBORNE, A. R., SERIO, M., RESIO, D., PUSHKAREV, A., ZAKHAROV, V. E. & BRANDINI, C. 2001 Freely decaying weak turbulence for sea surface gravity waves. *Phys. Rev. Lett.* **89**, 144501.
- PEREGRINE, D. H. 1976 Interaction of water waves and currents. *Adv. Appl. Mech.* **16**, 9–117.
- PEREGRINE, D. H. & SMITH, R. 1979 Nonlinear effects upon waves near caustics. *Phil. Trans. R. Soc. Lond. A* **292**, 341–370.
- SOCQUET-JUGLARD, H., DYSTHE, K. B., TRULSEN, K., KROGSTAD, H. E. & LIU, J. 2005 Probability distributions of surface gravity waves during spectral changes. *J. Fluid. Mech.* **542** 195–216.
- STEWARTSON, K. 1977 On the resonant interaction between a surface wave and a weak surface current. *Mathematika* **24**, 37–49.
- STOCKER, J. D. & PEREGRINE, D. H. 1999 The current-modified nonlinear Schrödinger equation. *J. Fluid Mech.* **399**, 335–353.
- TAYFUN, M. A. 1980 Narrow-band nonlinear sea waves. *J. Geophys. Res.* **85**, 1548–1552.
- TRULSEN, K. & DYSTHE, K. B. 1996 A modified nonlinear Schrödinger equation for broader bandwidth gravity waves on deep water. *Wave Motion* **24**, 281–289.
- TURPIN, F.-M., BENMOUSSA, C. & MEI, C. C. 1983 Effects of slowly varying depth and current on the evolution of a Stokes wavepacket. *J. Fluid Mech.* **132**, 1–23.
- WHITE, B. S. & FORNBERG, B. 1998 On the chance of freak waves at sea. *J. Fluid Mech.* **335**, 113–138.
- WHITE, B. S. 1999 Wave action on currents with vorticity. *J. Fluid Mech.* **386**, 329–344.
- WU, C. H. & YAO, A. 2004 Laboratory measurements of limiting freak waves on currents. *J. Geophys. Res.* **109**, C12002.
- ZAKHAROV, V. E. 1968 Stability of periodic waves of finite amplitude on the surface of a deep fluid. *J. Appl. Mech. Tech. Phys.* **9**, 86–94.